

# Vector solitons and dispersive waves in birefringent optical fibers

PRANNAY BALLA AND GOVIND P. AGRAWAL\* 

The Institute of Optics, University of Rochester, Rochester, New York 14627, USA

\*Corresponding author: govind.agrawal@rochester.edu

Received 2 April 2018; revised 16 July 2018; accepted 9 August 2018; posted 9 August 2018 (Doc. ID 327403); published 29 August 2018

We develop a general formalism for investigating the evolution of arbitrarily polarized short pulses inside a birefringent optical fiber. We use it to numerically study the formation of a dispersive wave inside fibers exhibiting medium to high birefringence when a short optical pulse is launched such that it propagates as a vector soliton. We also investigate the polarization evolution of both the vector soliton and dispersive wave generated by it. The results show that, while the polarization of the dispersive wave is controlled by linear birefringence of the fiber, polarization of the vector soliton is affected considerably by the nonlinear birefringence. The coupled nonlinear equations that we solve include both the Raman and Kerr nonlinearities. Moreover, they include the cross-polarization Raman terms that couple the orthogonally polarized components of the vector soliton. Polarization of the vector soliton is found to be affected considerably by the Raman nonlinearity in the case of medium birefringence. © 2018 Optical Society of America

**OCIS codes:** (190.4370) Nonlinear optics, fibers; (190.5530) Pulse propagation and temporal solitons.

<https://doi.org/10.1364/JOSAB.35.002302>

## 1. INTRODUCTION

It is well known that short optical pulses, propagating as temporal solitons inside an optical fiber, shed some energy in the form of a dispersive wave (DW) when perturbed by third-order dispersion (TOD) [1–5]. Indeed, such DWs and their trapping by solitons play a crucial role when optical fibers are used for supercontinuum generation [3–5]. DWs are also produced in birefringent optical fibers where the vector nature of optical solitons becomes important. However, most studies are based on the use of a scalar nonlinear Schrödinger (NLS) equation with only few exceptions [6–10]. Here, we use the term vector soliton in its broad sense, recalling that such solitons are in fact solitary waves.

Several fundamental questions emerge when we consider the perturbation of vector solitons inside birefringent optical fibers. A vector soliton consists of two orthogonally polarized components that move at a common speed by shifting their spectra to compensate for polarization-mode dispersion of the fiber. When such an entity is perturbed, it is not clear whether both components generate their own DWs at two distinct frequencies or if a single DW is created at a specific frequency. Furthermore, the initial state of polarization (SOP) of the DW is not obvious. It may coincide with the soliton's SOP, or it may lie far from that if each component of the vector soliton sheds its own DW. One may also ask how SOPs of the vector soliton and DWs evolve inside the optical fiber.

Depending on whether the DW is trapped or not by the vector soliton, its polarization evolution may exhibit different features.

In this study, we answer these questions by numerically investigating the generation of DWs inside birefringent optical fibers when an intense pulse is launched such that it propagates as a vector soliton. The coupled NLS equations that we solve include all relevant effects, including the cross-polarization (intermodal) Raman scattering. In Section 2, we provide the coupled NLS equations and discuss other mathematical details. In Section 3, we solve them numerically but ignore the Raman effects to focus on the Kerr-induced polarization dynamics of vector solitons and DWs. We discuss the general case in Section 4 by including the Raman effects and compare the results with those in Sections 3 to isolate the Raman-induced features. Section 5 is devoted to polarization instability, and the results are summarized in Section 6.

## 2. NUMERICAL MODEL

We consider a single-spatial-mode fiber with a stressed core such that it supports two orthogonally polarized modes with the same spatial profile but different propagation constants, denoted by  $\beta_x(\omega)$  and  $\beta_y(\omega)$ . An optical pulse is launched into this fiber with an initial SOP such that both polarization components are excited simultaneously and form a vector soliton. By expanding  $\beta_x(\omega)$  and  $\beta_y(\omega)$  in a Taylor series around the

pulse's central frequency  $\omega_0$  and following a standard procedure [5], we write the total electric field as

$$\mathbf{E}(\mathbf{r}, t) = \text{Re}(\hat{x}A_x e^{i(\beta_{0x} - i\omega_0 t)} + \hat{y}A_y e^{i(\beta_{0y} - i\omega_0 t)}) \quad (1)$$

and obtain the following two coupled NLS equations for the slowly varying envelope amplitudes  $A_j(z, t)$  ( $j = x, y$ ):

$$\frac{\partial A_j}{\partial z} + \beta_{1j} \frac{\partial A_j}{\partial t} + \frac{i\beta_2}{2} \frac{\partial^2 A_j}{\partial t^2} - \frac{\beta_3}{6} \frac{\partial^3 A_j}{\partial t^3} = Q_j, \quad (2)$$

where we retained the dispersive terms up to the third order, included different group delays of the two polarization modes through  $\beta_{1j}$ , and assumed  $\beta_2$  and  $\beta_3$  to be the same for them. It is important to include the TOD through  $\beta_3$  as it controls the DW generation. The difference of  $\beta_{1x} - \beta_{1y}$  represents the differential group delay (DGD) of a birefringent fiber.

The nonlinear terms  $Q_x$  and  $Q_y$  include both the Kerr and Raman contributions. Before writing them, we convert these equations into a dimensionless form by using the so-called soliton units [5]:

$$\begin{aligned} \tau &= (t - \bar{\beta}_1 z) / T_0, & \xi &= z / L_D, \\ A_x &= u \sqrt{P_0} e^{-i\Delta\beta z/2}, & A_y &= v \sqrt{P_0} e^{i\Delta\beta z/2}, \end{aligned} \quad (3)$$

where  $T_0$  and  $P_0$  are the width and the peak power of input pulses,  $\bar{\beta}_1 = (\beta_{1x} + \beta_{1y})/2$  is the average group delay,  $L_D = T_0^2/|\beta_2|$  is the dispersion length of the fiber, and  $\Delta\beta = \beta_{0x} - \beta_{0y} = (\omega_0/c)\Delta n$  is related to fiber's birefringence. The resulting coupled NLS equations take the form

$$i \left( \frac{\partial u}{\partial \xi} + \delta \frac{\partial u}{\partial \tau} \right) + bu + \frac{1}{2} \frac{\partial^2 u}{\partial \tau^2} + i\delta_3 \frac{\partial^3 u}{\partial \tau^3} = Q_x L_D, \quad (4)$$

$$i \left( \frac{\partial v}{\partial \xi} - \delta \frac{\partial v}{\partial \tau} \right) - bv + \frac{1}{2} \frac{\partial^2 v}{\partial \tau^2} + i\delta_3 \frac{\partial^3 v}{\partial \tau^3} = Q_y L_D, \quad (5)$$

where we have introduced three dimensionless parameters

$$\begin{aligned} b &= \frac{T_0^2(\Delta\beta)}{2|\beta_2|}, & \delta &= \frac{T_0}{2|\beta_2|}(\beta_{1x} - \beta_{1y}), \\ \delta_3 &= \frac{\beta_3}{6|\beta_2|T_0}, \end{aligned} \quad (6)$$

and the two nonlinear terms are given by [7–9]

$$\begin{aligned} Q_x &= \frac{iN^2}{L_D} \left( 1 + \frac{i}{\omega_0} \frac{\partial}{\partial t} \right) \left[ (1 - f_R) \left( |u|^2 u + \frac{2}{3} |v|^2 u + \frac{1}{3} v^2 u^* \right) \right] \\ &+ f_R (u [b_1 \otimes |u|^2 + b_2 \otimes |v|^2] + v [b_3 \otimes (uv^* + vu^*)]), \end{aligned} \quad (7)$$

$$\begin{aligned} Q_y &= \frac{iN^2}{L_D} \left( 1 + \frac{i}{\omega_0} \frac{\partial}{\partial t} \right) \left[ (1 - f_R) \left( |v|^2 v + \frac{2}{3} |u|^2 v + \frac{1}{3} u^2 v^* \right) \right] \\ &+ f_R (v [b_1 \otimes |v|^2 + b_2 \otimes |u|^2] + u [b_3 \otimes (uv^* + vu^*)]), \end{aligned} \quad (8)$$

where  $\otimes$  represents the convolution operation, and  $N = \sqrt{\gamma P_0 L_D}$  is the soliton number. The last Raman term in Eqs. (7) and (8) involving  $b_3$  represents the contribution of cross-polarization (intermodal) Raman scattering.

The Raman model used for vector solitons is different from the Blow–Wood model commonly used in a scalar theory [11]. The main difference is that we include both the isotropic and anisotropic parts of the nuclear response through three time-dependent functions defined as [12,13]

$$h_1(t) = (f_a + f_c)h_a(t) + f_b h_b(t), \quad h_2(t) = f_a h_a(t), \quad (9)$$

$$h_3(t) = [f_c h_a(t) + f_b h_b(t)]/2, \quad (10)$$

where  $h_a(t)$  and  $h_b(t)$  represent the isotropic and anisotropic parts of the nuclear response and are given by [11–13]

$$h_a(t) = \frac{\tau_1^2 + \tau_2^2}{\tau_1 \tau_2^2} \exp\left(-\frac{t}{\tau_2}\right) \sin\left(\frac{t}{\tau_1}\right), \quad (11)$$

$$h_b(t) = [(2\tau_b - t)/\tau_b^2] \exp(-t/\tau_b), \quad (12)$$

with  $f_a = 0.75$ ,  $f_b = 0.21$ , and  $f_c = 0.04$ . The three time scales are  $\tau_1 = 12.2$  fs,  $\tau_2 = 32$  fs, and  $\tau_b = 96$  fs for silica fibers. The parameter  $f_R$  provides the fractional contribution of the delayed Raman response. Its value  $f_R = 0.245$  for silica is different from that used in the Blow–Wood model and was found in Ref. [13] by fitting the Raman gain curve.

Before solving Eqs. (4) and (5) numerically, we discuss their soliton-like solutions briefly. Since these equations are not integrable by the inverse scattering method, steady-state vector solitons do not exist. Even when one neglects all higher-order terms (related to self-steepening, TOD, and the Raman nonlinearity) and retains only the Kerr nonlinearity, the soliton-like solutions of Eqs. (4) and (5) have not been found. A specific soliton solution has been reported in the special case of a pulse polarized linearly at  $45^\circ$  from the slow axis and propagating inside a high-birefringence fiber [14], but only after neglecting the four-wave mixing (FWM) term in Eqs. (7) and (8). For this reason, we focus on the situation first considered by Menyuk [15], in which an optical pulse is polarized linearly at a finite angle from the slow axis and is launched into a birefringent fiber with sufficient energy that the soliton order  $N$  is close to 1. It was found that the  $x$  and  $y$  components of such a pulse shift their spectra such that they trap each other and move at a common speed. Our objective is to study how this trapping is affected by the higher-order terms in Eqs. (4) and (5) related to the TOD and Raman nonlinearity.

More specifically, we solve the coupled NLS Eqs. (4) and (5) numerically with an input in the form

$$u(0, \tau) = \cos \theta \text{sech}(\tau), \quad v(0, \tau) = \sin \theta \text{sech}(\tau) e^{i\psi}, \quad (13)$$

where the angles  $\theta$  and  $\psi$  characterize the SOP of the vector soliton. We choose the initial SOP of the input pulse to be linear ( $\psi = 0$ ) and take  $\theta = 45^\circ$  so that the  $x$  and  $y$  components of the soliton are equally intense. Parameter  $N$  is related to the peak power of input pulses; a fundamental soliton forms for  $N$  in the range of 0.5 to 1.5. We decided to use  $N = 1.4$  because the amplitude of the DWs is enhanced for this value without complications arising from soliton fission [5]. For numerical simulations, we use a relatively wide temporal window ( $-200 < \tau < 200$ ) with  $2^{14}$  points in the time domain. However, the coupled NLS equations are solved in

the frequency domain using the Runge–Kutta method with an adjustable step size along the fiber length [16].

The birefringence parameters  $b$  and  $\delta$  are fiber specific and can vary over a wide range. We decided to focus on two cases of medium and high birefringence. In the former case, we take  $b = 0.1$  and  $\delta = 0.1$ , but increase these values to  $b = 10$  and  $\delta = 1$  in the high-birefringence case. It is often argued that  $b$  can be set to zero in the case of high birefringence because of an averaging effect produced by rapid changes in the relative phase of the two polarization components [5]. We decided not to do so to reveal the residual effects when  $b$  is not too large. The only other parameter we need is  $\delta_3$ , taken to be  $\delta_3 = 0.1$ . The numerical values of all parameters used in our numerical work are appropriate for silica fibers when  $\sim 100$  fs pulses are launched at a wavelength near 1550 nm.

To characterize the SOP evolution, we trace the trajectory of the Stokes vector on the Poincaré sphere. However, the SOP can be nonuniform in time at a given distance while also varying along the fiber length. To focus on length variations, the SOP at the intensity peak is used for both the DW and the vector soliton after isolating them through spectral filtering. The magnitude  $S_0$  and the components of the Stokes vector are calculated using the definitions [5]

$$S_0 = |A_x|^2 + |A_y|^2, \quad S_1 = |A_x|^2 - |A_y|^2, \quad (14)$$

$$S_2 = 2 \operatorname{Re}(A_x A_y^*), \quad S_3 = -2 \operatorname{Im}(A_x A_y^*). \quad (15)$$

We map the sphere onto a two-dimensional plane using the Hammer projection. We first find the longitude  $\phi$  and latitude  $\chi$  using  $\tan(2\phi) = S_2/S_1$  and  $\sin(2\chi) = S_3/S_0$  and then calculate the coordinates for the Hammer projection using [17]

$$x_h = \frac{2\sqrt{2} \cos(2\chi) \sin(\phi)}{\sqrt{1 + \cos(2\chi) \cos(\phi)}}, \quad y_h = \frac{\sqrt{2} \sin(2\chi)}{\sqrt{1 + \cos(2\chi) \cos(\phi)}}. \quad (16)$$

We use this projection to visualize the entire Poincaré sphere in a single plot, thus avoiding two separate plots displaying the front and back of the Poincaré sphere.

### 3. EVOLUTION WITHOUT RAMAN NONLINEARITY

In this section, we simplify the problem by setting  $f_R = 0$  so that the Raman contribution to the nonlinear response is not included. This case allows us to gain physical insight into the soliton dynamics in the presence of the Kerr nonlinearity alone. This helps us in interpreting the results of the next section where the Raman contribution is included.

#### A. Fibers with Medium Birefringence

The top row of Fig. 1 shows the temporal evolution of the vector soliton inside the fiber by plotting  $|u(\xi, \tau)|^2$  and  $|v(\xi, \tau)|^2$  [on a color-coded decibel (dB) scale] over 25 dispersion lengths ( $\xi = 0-25$ ). The middle row shows the spectral evolution under the same conditions, and the bottom row shows the spectrograms of the two polarization components at a distance  $\xi = 20$ . As expected, the two components of the vector soliton move at the same speed in spite of a group-velocity mismatch resulting from the DGD (included through the parameter  $\delta$ ).

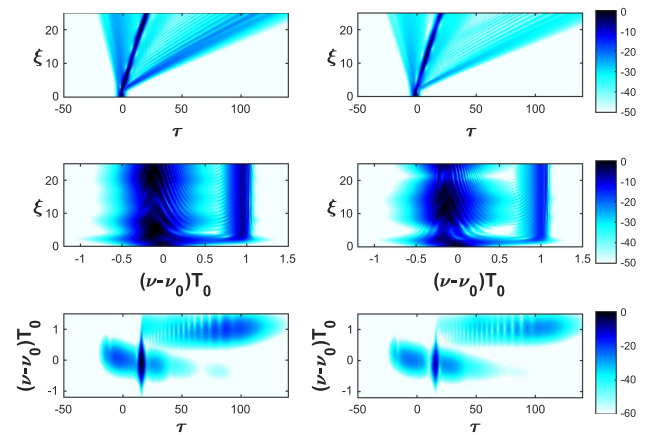


**Fig. 1.** Temporal (top row) and spectral (middle row) evolution over  $25L_D$  for the  $x$  (left) and  $y$  components of a vector soliton ( $N = 1.4$ ) excited by launching a linearly polarized pulse ( $\theta = 45^\circ$ ) into a medium-birefringence fiber ( $b = 0.1$ ,  $\delta = 0.1$ ). The bottom row shows the spectrograms of the two polarization components at a distance  $\xi = 20$ . The color bar shows the relative intensity on a decibel scale.

This is a consequence of the cross-phase modulation (XPM) that shifts the pulse spectra in the opposite directions such that the two components trap each other and move at a common speed [15]. Tilting of the soliton trajectory toward the right is due to the TOD effects included through  $\delta_3 = 0.1$ . We have verified that a left tilt occurs for  $\delta_3 = -0.1$ , and no tilt occurs for  $\delta_3 = 0$ . The temporal and spectral oscillations seen in Fig. 1 are related to changes in the SOP of the vector soliton discussed later.

Our numerical simulations include TOD, which perturbs the vector soliton and forces it to shed some energy in the form of DWs. As seen in Fig. 1, DWs are generated within the first few dispersion lengths at a blue-shifted frequency corresponding to the spectral peaks located near  $(\nu - \nu_0)T_0 = 1$ . Even though the spectra of the two DWs overlap to a large extent, their central frequencies differ by a small amount, indicating that the  $x$  and  $y$  components of the vector soliton emit their own DWs. However, one can think of them as the two polarization components of a single DW. As seen in Fig. 1, the two components have different amplitudes (the  $y$  component is less intense compared to the  $x$  component), indicating that the SOP of the DW is different from that of the vector soliton.

Similar to the case of scalar solitons, perturbation theory and a phase-matching condition can be used to predict the frequencies of the orthogonally polarized DWs [10,18]. We derive approximate analytical expressions of these frequencies in Appendix A. They show that the frequencies of the two DW components are different because of the DGD induced by the fiber's birefringence, and the magnitude of the frequency difference is governed by the parameter  $\delta$  defined in Eq. (6). Our numerical results agree with the analytical predictions.

Figure 1 also shows that a small fraction of pulse energy is left at the original location of the input pulse. This part cannot form a soliton and spreads temporally appearing on the left side of the soliton in the top row. Its presence is clearly evident in

the spectrograms where we see tails on both sides of the soliton. In the following, we refer to this part at the original frequency as pulse remnants. It should be distinguished from the DW generated through TOD that is blue-shifted and appears on the right side of the soliton.

An interesting question is how the SOP of the vector soliton and that of the DW associated with it evolves inside the fiber. Even though the spectral peaks of the  $x$  and  $y$  components for the soliton and the DW do not coincide exactly, their spectra overlap. As a result, in the time domain, both the soliton and the DW are vectorial in nature, and their temporal peaks have a well-defined SOP that evolves along the fiber length. Figure 2(a) shows how the SOP evolves along the fiber for the vector soliton, DW, and pulse remnants. Even though the SOP of all three entities changes with propagation, the resulting evolution patterns are quite distinct for them. It turns out that the SOP evolution can be understood qualitatively using the theory developed for a continuous wave (CW) beam. In this theory, the Stokes vector evolves as [5,19]

$$d\mathbf{S}/dz = \mathbf{W} \times \mathbf{S}, \quad \mathbf{W} = \Delta\beta\hat{x} - 2\gamma(S_3/3)\hat{z}. \quad (17)$$

The preceding equation shows that the Stokes vector rotates on the Poincaré sphere around an axis oriented along the vector  $\mathbf{W}$  that has a linear part and a nonlinear part. The linear birefringence forces  $\mathbf{S}$  to rotate around the  $x$  axis, while the nonlinear birefringence forces it to rotate around the  $z$  axis. In the case of medium birefringence, the two rotations compete, leading to the patterns seen in Fig. 2(a).

Consider first SOP of the vector soliton that starts linearly polarized at  $\theta = 45^\circ$  (marked by an arrow in Fig. 2). The SOP soon becomes slightly elliptical and moves toward the center as energy is transferred from  $A_y$  to  $A_x$ . In the absence of the nonlinear effects, it will move in a circular pattern around the center. However, the linear and nonlinear rotations are comparable in magnitude in the case of medium birefringence, leading to the pattern seen in Fig. 2(a). Physically, nonlinear polarization rotations are induced by the XPM and FWM effects that couple to the two polarization components in a nonlinear fashion [5]. The SOPs of both the DW and pulse remnants move in a circular fashion around the center, as expected from linear birefringence. The SOP of the DW does not coincide initially with that of the soliton (because the amplitude of its  $y$  component is smaller compared to the  $x$  component) and lies close to the center in Fig. 2(a).

### B. Fibers with High Birefringence

Figure 3 shows the temporal (top row) and spectral (middle row) evolutions of the two polarization components in the case of a fiber with high birefringence by choosing  $b = 10$  and  $\delta = 1$ . All other parameters remain the same. It should be compared with the case of medium birefringence shown in Fig. 1. The differences in the two cases are quite remarkable and stem mostly from the larger DGD between the  $x$  and  $y$  components. More specifically, a relatively large difference in the group velocities of the two components destroys their mutual trapping. Only a small fraction of energy of the  $y$  component is trapped by the  $x$  component to form a vector soliton. The remaining part forms a scalar soliton that remains polarized along the  $y$

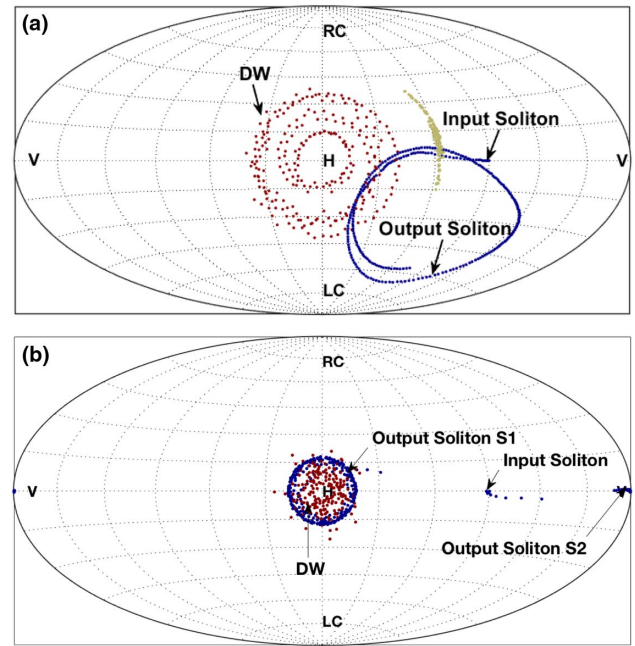


**Fig. 2.** SOP evolution for the vector soliton (solid blue), DW (dotted red), and pulse remnants (gray) in a fiber with (a) medium or (b) high birefringence. In the Hammer projection, the longitude and latitude lines are  $15^\circ$  apart, with H and V marking horizontal and vertical linear SOPs and the poles representing circular SOPs. In the high-birefringence case, S2 is the scalar soliton polarized along the  $y$  axis.

axis, moves faster than the vector soliton, and appears on the left side in the temporal trace in Fig. 3. The two faint vertical spectral lines on the right side in Fig. 3 correspond to the two DWs emitted by the two temporal parts of the  $y$  component (the V pattern seen on the top). The spectrograms at a distance  $\xi = 20$  in the bottom row of Fig. 3 make these features even more explicit. On the left side, one sees a single soliton with a relatively intense DW; in contrast, on the right side, we see two solitons and two much weaker DWs emitted by them and moving at different speeds.

The SOP evolution in the high-birefringence case is shown in Fig. 2(b), and it should be compared to the low-birefringence case shown in Fig. 2(a). Once again, note the dramatic changes induced by the larger values of the parameters  $b$  and  $\delta$ . The initial SOP of the vector soliton (marked by an arrow) changes very quickly as it moves toward the center and rotates in a circular fashion around it (blue curve). The SOP of the DW (red dots) also evolves in a nearly circular fashion close to that of the vector soliton. The SOP of the scalar soliton does not change and lies at the location marked V, because this soliton remains polarized along the  $y$  axis. All of these features can be understood qualitatively from Eq. (17). In the case of high birefringence, the linear part of the vector  $\mathbf{W}$  dominates compared to the nonlinear part and forces the SOP to rotate around the  $x$  axis (normal to the plane of the figure). This is the reason why both the vector soliton and DWs follow a circular path around the center in Fig. 2(b).

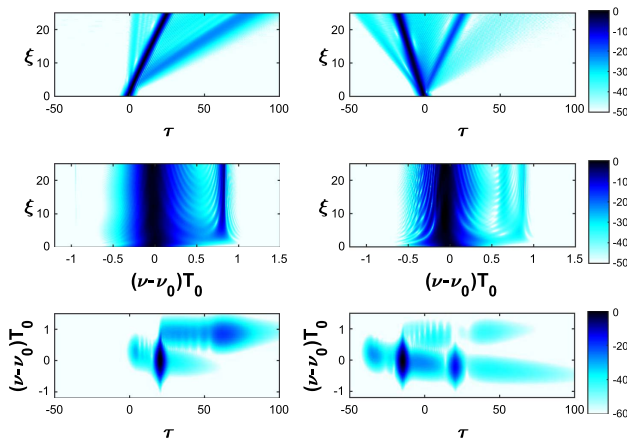


**Fig. 3.** Same as Fig. 1 except for a fiber with high birefringence ( $b = 10$  and  $\delta = 1$ ).

#### 4. EVOLUTION WITH RAMAN NONLINEARITY

In this section, we consider the full problem and include both the Kerr and Raman contributions to the nonlinear response. While the Raman contribution is relatively small when the input pulse width exceeds 1 ps, it must be included for shorter femtosecond pulses. We have chosen  $T_0 = 100$  fs, which corresponds to a full width at half-maximum of 176 fs for the input pulse.

##### A. Fibers with Medium Birefringence

Figure 4 shows the temporal (top row) and spectral (middle row) evolutions over 25 dispersion lengths ( $\xi = 0-25$ ) inside a fiber with medium birefringence together with the spectrograms at  $\xi = 20$  for the  $x$  (left column) and  $y$  (right column) components of the pulse. It should be compared with Fig. 1. In both cases, the two polarization components trap each other through XPM and move at a common speed as a vector soliton. Indeed, temporal evolutions look quite similar when the Raman effects are included, except for a larger tilt of the soliton trajectories toward the right, indicating a slow down of the vector soliton. This is expected, since the main effect of the Raman contribution is to shift the pulse spectrum toward the red side, the so-called soliton self-frequency shift (SSFS), that leads to a reduced group velocity. Indeed, the pulse spectra in the middle row exhibit such a red shift. Notice that the SSFS is in addition to the XPM-induced spectral shifts of the two polarization components on the red and blue sides required for soliton trapping to occur. For this reason, the spectra are not identical for the two polarization components.

Figure 5 compares the shapes and spectra of output pulses at  $\xi = 25$  for the  $x$  (left column) and  $y$  (right column) components with (blue) and without (red) the Raman contribution. In the temporal traces, the narrow central peak corresponds to the vector soliton, and the broad peak on the right corresponds to the DW emitted by it. One sees clearly that the vector soliton moves slower when the Raman effects are included. The corresponding spectral traces show that this is due to a red shift (SSFS) through intrapulse Raman scattering. The spectra of DWs (narrower peaks on the right side) are not affected by

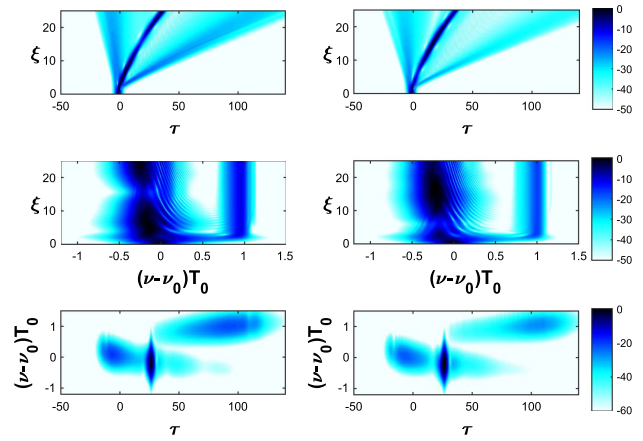


**Fig. 4.** Same as Fig. 1 except for including the Raman contribution. The optical fiber has medium birefringence ( $b = 0.1$  and  $\delta = 0.1$ ).

SSFS, but their different amplitudes indicate that the  $x$  component of the DW is more intense compared to the  $y$  component.

One may ask whether the Raman contribution affects the SOP of the vector soliton. Figure 6(a) shows how the SOP evolves along the fiber for the vector soliton, DW, and pulse remnants when both the Kerr and Raman contributions are included. It should be compared with Fig. 2(a) where the Raman contribution was ignored. It is evident that the SOP of the vector soliton exhibits an evolution pattern that is quite different when the Raman effects are included. The initial evolution of the vector soliton's SOP is similar in the sense that the SOP becomes elliptically polarized and moves toward the center, but the SSFS changes the SOP in such a fashion that its trajectory covers the entire Poincaré sphere, in sharp contrast with the case of purely Kerr nonlinearity. The SOPs of the pulse remnants and that of the DW still move in a circular fashion around the center. This is expected because these two evolve linearly, as dictated by the linear birefringence, and are not affected by the Raman effects. We remark that one cannot

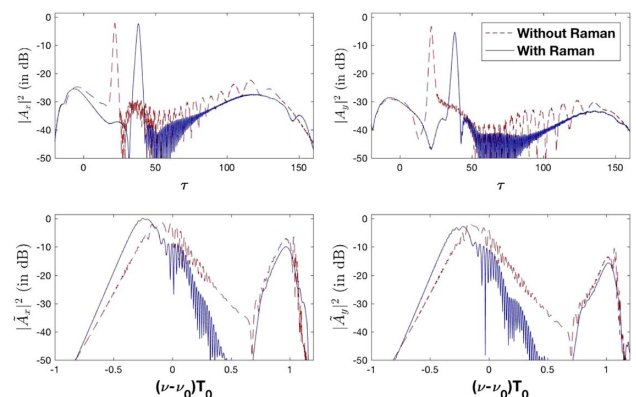


**Fig. 5.** Temporal (top) and spectral (bottom) intensity profiles at a distance of  $\xi = 25$  for the  $x$  (left column) and  $y$  (right column) polarization components with (solid blue) and without (dashed red) the Raman contribution. Both spectra are red-shifted but differ from each other because of different XPM-induced spectral shifts.

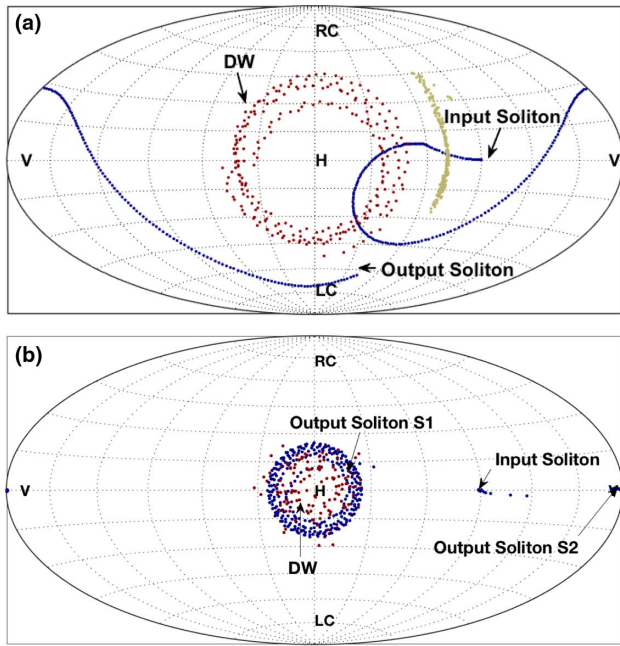


**Fig. 6.** Same as Fig. 2 except the Raman contribution is included in the cases of both (a) medium and (b) high birefringence.

use the CW theory to understand these SOP changes because the SSFS occurs only for short optical pulses.

### B. Fibers with High Birefringence

As the last case, we consider the impact of Raman nonlinearity in fibers exhibiting high birefringence. Figure 7 shows the temporal (top row) and spectral (middle row) evolutions of the two polarization components by choosing  $b = 10$  and  $\delta = 1$ . It should be compared with Fig. 3, where the case of high birefringence is shown without the Raman contribution. In contrast with the medium-birefringence case, only minor changes occur when the Raman term is included. In both cases, a relatively large difference in the group velocities of the two components destroys their mutual trapping. Only a small fraction of energy of the  $y$  component is trapped by the  $x$  component to form a vector soliton. The remaining energy forms a scalar soliton that moves faster than the vector soliton. Both temporal components still emit DWs, as seen in the middle row of Fig. 3, where two vertical lines show the frequencies of two DWs emitted by these two temporal parts of the  $y$  component moving at different speeds. The Raman-induced SSFS still occurs, but it has a relatively minor effect on the evolution process.

The SOP evolution in the high-birefringence case is shown in Fig. 6(b), and it should be compared to the low-birefringence case shown in Fig. 6(a), but also to the high-birefringence case in Fig. 2(b), where the Raman effects were excluded. The high birefringence affects the SOP evolution drastically, but the Raman effects do not introduce dramatic changes. Indeed, the SOP evolution appears to be dominated by the large linear birefringence of the fiber (or by the relatively large values of the parameters  $b$  and  $\delta$ ). The initial SOP of the vector soliton (blue curves) changes very quickly and rotates in a circular fashion around the center. The SOP of the DW (red dots) also

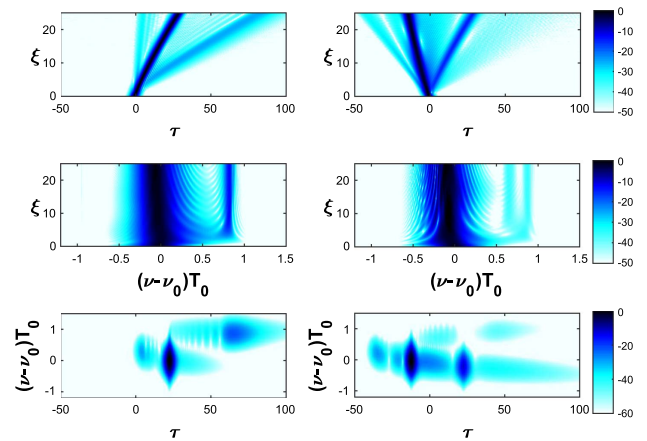


**Fig. 7.** Same as Fig. 3 except that the Raman contribution is included. The fiber's high birefringence is included by choosing  $b = 10$  and  $\delta = 1$ .

evolves in a nearly circular fashion. We conclude that the intra-pulse Raman scattering does not have a significant effect in the presence of high birefringence. It causes a red shift in the spectra of both components, but the impact of that red shift on the SOP evolution of the soliton is relatively minor.

### 5. POLARIZATION INSTABILITY

One may ask how the results change when the initial SOP of the input pulse is different from the  $45^\circ$  orientation considered so far. We carried out a large number of simulations for different initial SOPs of the input pulse on the Poincaré sphere. The results remain qualitatively similar as long as the input SOP is not oriented close to the fast axis of the fiber. When  $\theta$  exceeds  $80^\circ$  such that most of the pulse energy is along the fast axis of the fiber, new qualitative features appear that are related to an instability known as polarization instability [5,20]. In our study, this instability occurs only in the medium-birefringence case because it requires the nonlinear length to be comparable to the beat length of the fiber. Our numerical results performed with  $\delta = 0.1$  show that a large fraction of input energy is transferred from the  $y$  component to the  $x$  component and then back to the  $y$  component of the pulse in a periodic fashion. Figure 8(a) shows changes in the fraction of input energy in the two polarization components over a distance of  $100L_D$  for  $\theta = 85^\circ$  (dashed curves) and  $89^\circ$  (solid curves) without including the Raman effects. Figure 8(b) shows the impact of including the Raman terms. As seen there, periodic energy transfer is reduced considerably for  $\theta = 85^\circ$  and almost ceases to occur for  $\theta = 89^\circ$  when the Raman effects are included. It appears that the spectral red shift of the soliton eliminates polarization instability to a large extent.

Another hallmark of polarization instability is that it leads to large variations in the soliton's SOP with small changes in the input and fiber parameters [5]. Figure 9 shows the polarization evolution of the DW and the soliton over  $100L_D$  for  $\theta = 85^\circ$  in a fiber with medium birefringence ( $b = 0.1$ ) with the Kerr nonlinearity alone. It should be compared with Fig. 2(a), where  $\theta = 45^\circ$  so that the energy is divided equally between the

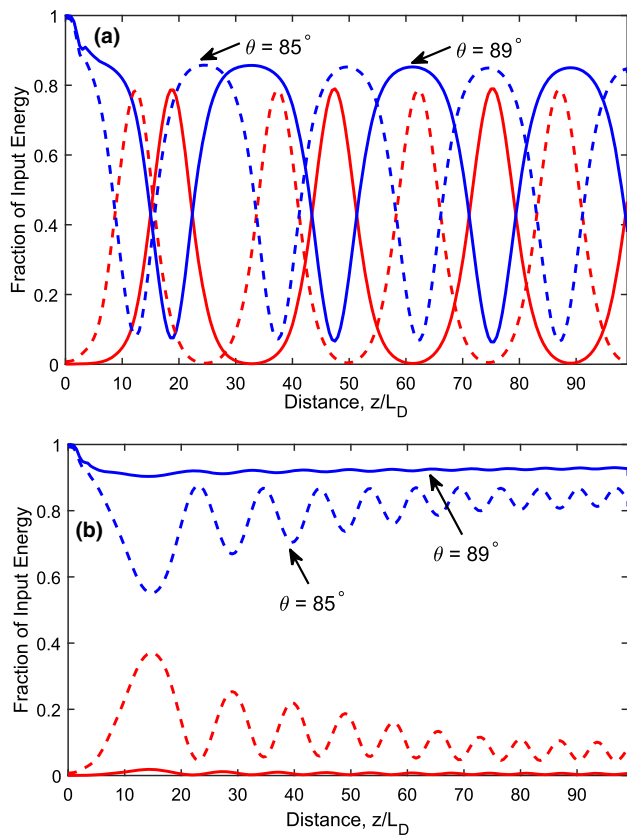


**Fig. 8.** Periodic energy transfer over a distance of  $100L_D$  for  $\theta = 85^\circ$  (dashed) and  $89^\circ$  (solid) (a) without and (b) with the Raman effects. The red and blue curves represent, respectively, the fraction of energy in the  $x$  and  $y$  components of the pulse. The fiber has medium birefringence with the same parameters as in Fig. 1.

$x$  and  $y$  components of the pulse. Whereas the DW remains polarized close to the fast axis (red dots), the SOP of the soliton (blue dots) moves over the entire Poincaré sphere with distance, in sharp contrast to the  $\theta = 45^\circ$  case. The same behavior occurs for  $\theta = 89^\circ$  and its other values close to the fast axis. As expected from the earlier discussion, the SOP evolution changes drastically when the Raman effects are included. We found that the soliton's SOP varied little and remained close to the fast axis of the fiber. The same behavior occurred for fiber with high birefringence.

## 6. CONCLUDING REMARKS

In this paper, we have developed a formalism for investigating the evolution of arbitrarily polarized short pulses inside a birefringent optical fiber. The theory includes both the Raman and Kerr nonlinearities, as well as higher-order dispersion terms, so that it can be used even when femtosecond pulses are launched inside the fiber. More specifically, the coupled nonlinear equations that we solve include the cross-polarization Raman scattering terms that couple the orthogonally polarized components of the pulse in addition to the XPM-induced coupling terms through the Kerr nonlinearity.

As a specific example, we used the coupled NLS equations to study evolution of a short optical pulse that is polarized linearly at  $45^\circ$  from the slow axis. When this pulse is launched in the

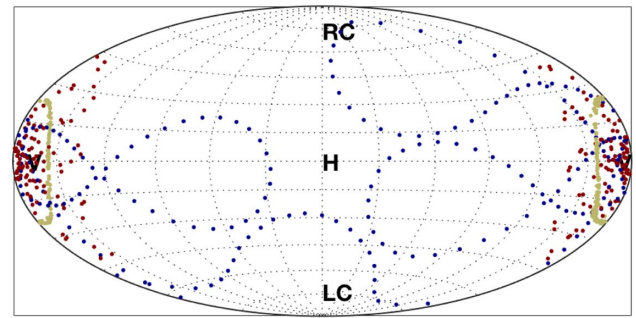


**Fig. 9.** Same as Fig. 2(a) except that  $\theta = 85^\circ$  so that the input pulse is polarized linearly close to the fast axis of a fiber with medium birefringence ( $b = 0.1$ ).

anomalous dispersion region of a medium-birefringence fiber, the XPM-induced nonlinear coupling between the  $x$  and  $y$  components creates a vector soliton that overcomes DGD through spectral shifts. Its SOP starts changing through a combination of linear and nonlinear birefringence, while it sheds radiation in the form of a DW because of TOD-induced perturbations. The  $x$  and  $y$  components of the DW have spectra that overlap substantially but peak at slightly different frequencies because of different dispersion relations associated with them. We numerically investigate the polarization evolution of both the vector soliton and the DW generated by it. The results show that while the DW polarization is controlled by the linear birefringence of the fiber, the SOP of the vector soliton is affected considerably by the nonlinear birefringence. Indeed, when we repeat the simulations for a high-birefringence fiber, it is the linear birefringence that controls the SOP of both the DW and the vector soliton. The Raman effects, important for short pulses, lead to an additional red shift of the spectra for both the  $x$  and  $y$  components, but they do not affect the formation of a vector soliton and the generation of DWs. The SOP of the vector soliton is found to be affected considerably by the Raman nonlinearity.

We also studied the impact of initial SOP of the soliton. Although quantitative details do differ, the qualitative behavior remains the same for nearly all SOPs of the input pulse, except when the pulse is polarized close to the fast axis. In this case, when the Raman effects are ignored (only Kerr nonlinearity is included) and the fiber has low-to-medium birefringence, almost the entire pulse energy is exchanged between the  $x$  and  $y$  components in a periodic fashion along the fiber length, and the SOP of the soliton moves over the entire Poincaré sphere in a wild fashion. Both of these effects are related to the onset of polarization instability. However, this instability almost disappears when the Raman effects are included or a fiber with high birefringence is considered. The main point to note is that the formalism developed in this paper can be used for an arbitrary SOP of the input pulse.

## APPENDIX A: FREQUENCY OF DISPERSIVE WAVES

The frequency shift  $\Omega$  of the DW emitted by a scalar soliton with the central frequency  $\omega_s$  is set by the phase-matching

condition  $\beta(\omega_s + \Omega) = \beta(\omega_s) + k_n$ , where  $k_n = \frac{1}{2}\gamma P_0$  represents the nonlinear contribution to the soliton's propagation constant [4,5]. A similar condition determines the frequency in the case of a vector soliton in birefringent fibers, except that we must apply this condition separately to the  $x$  and  $y$  polarization components of the vector soliton. The corresponding frequency shifts are governed by

$$\beta_x(\omega_{sx} + \Omega_x) = \beta_x(\omega_{sx}) + k_{nx}, \quad (\text{A1})$$

$$\beta_y(\omega_{sy} + \Omega_y) = \beta_y(\omega_{sy}) + k_{ny}. \quad (\text{A2})$$

The nonlinear contributions  $k_{nx}$  and  $k_{ny}$  are ignored in what follows, since they play a relatively minor role in the scalar case [5] and may do so even in the vector case.

To calculate  $\Omega_x$  and  $\Omega_y$ , we expand  $\beta_j(\omega_{sj} + \Omega_j)$  with  $j = x, y$  in a Taylor series and take into account that the vector soliton moves at a common group velocity set by  $v_g^{-1} = \beta_{1s} = \frac{1}{2}(\beta_{1x} + \beta_{1y})$ . Keeping terms up to the third order in the Taylor expansion, the DW frequencies are obtained from the equations

$$\frac{1}{6}\beta_3\Omega_x^2 + \frac{1}{2}\beta_2\Omega_x + \frac{1}{2}\Delta\beta_1 = 0, \quad (\text{A3})$$

$$\frac{1}{6}\beta_3\Omega_y^2 + \frac{1}{2}\beta_2\Omega_y - \frac{1}{2}\Delta\beta_1 = 0, \quad (\text{A4})$$

where  $\Delta\beta_1 = \beta_{1x} - \beta_{1y}$  is the DGD between the two polarization components. These quadratic equations can easily be solved to obtain  $\Omega_x$  and  $\Omega_y$ , and the result is

$$\Omega_{x,y} = -\frac{3\beta_2}{2\beta_3} \left( 1 + \sqrt{1 \mp \frac{4\beta_3\Delta\beta_1}{3\beta_2^2}} \right). \quad (\text{A5})$$

This result is similar to that obtained by Conforti and Trillo in the case of optical wave breaking in normal group-velocity dispersion (GVD) fibers [21].

To make a comparison with the numerical simulations, it is useful to write Eq. (A5) in a normalized form in terms of the parameters defined in Eq. (6). Recalling that  $\beta_2 < 0$  for a soliton, the result is

$$\Omega_{x,y}T_0 = \frac{1}{4\delta_3} \left( 1 + \sqrt{1 \mp 16\delta\delta_3} \right). \quad (\text{A6})$$

In the case of fibers with low to medium birefringence, typically  $16\delta\delta_3 \ll 1$ , and the frequencies can be approximated as

$$\Omega_{x,y}T_0 = \frac{1}{2\delta_3} \mp 2\delta. \quad (\text{A7})$$

However, this approximation may not work for fibers with high birefringence. For example, when  $\delta_3 = 0.1$  and  $\delta = 1$ , the quantity  $16\delta\delta_3$  exceeds one, and the frequency shift becomes complex when negative sign is chosen in Eq. (A6). This issue may be resolved when the nonlinear contribution to the soliton's propagation constant is included.

Equation (A7) is applicable for medium-birefringence fibers. The first term provides the dominant contribution to the frequency shift and is identical to the scalar result. The second term in this equation shows that the DGD changes

frequencies slightly in the opposite directions for the  $x$  and  $y$  components. To compare with the numerical simulations, we use  $\delta_3 = 0.1$  and  $\delta = 0.1$ . Since  $\Omega_{x,y}T_0 = 5 \mp 0.2$ , it is easy to conclude that birefringence-induced changes in the DW frequencies are relatively small. For comparing these values with numerics, we recall that  $\Omega_j$  with  $j = x, y$  is the shift relative to the soliton frequency  $\omega_{sj}$ , which is itself shifted from the input central frequency  $\omega_0$  by an amount that depends on  $\delta$ . Accounting for it and dividing  $\Omega_j$  by  $2\pi$ , the predicted values are  $(\nu_j - \nu_0)T_0 = 0.800 \mp 0.016$  for  $j = x$  and  $y$ , respectively. Numerical values must be obtained from the DW spectra shown in Fig. 5 by the dashed curve. Since both of these spectra are relatively broad and asymmetric, it is not obvious what frequency should be compared with the theoretical value. If we use the center frequency of each spectrum, the predictions of Eq. (A7) are in reasonable agreement with the numerical simulations when the Raman effects are ignored. In the high-birefringence case, the DW spectrum is narrower, and its center frequency is indeed close to  $(\nu - \nu_0)T_0 = 0.8$  for the  $x$  component in Fig. 4.

The situation becomes more complicated when intrapulse Raman scattering induces an additional red shift of the soliton spectrum. Since the group velocity of the soliton changes, the frequency of the DW also shifts. The solid curves in Fig. 4 show the DW spectra in this situation. Comparing it with the dashed curves obtained without the Raman terms, we conclude that Raman-induced spectral changes to the DW are relatively minor.

**Funding.** National Science Foundation (NSF) (ECCS-1505636).

## REFERENCES

1. P. K. A. Wai, H. H. Chen, and Y. C. Lee, "Radiations by solitons at the zero group-dispersion wavelength of single-mode optical fibers," *Phys. Rev. A* **41**, 426–439 (1990).
2. N. Akhmediev and M. Karlsson, "Cherenkov radiation emitted by solitons in optical fibers," *Phys. Rev. A* **51**, 2602–2607 (1995).
3. J. M. Dudley, G. Genty, and S. Coen, "Supercontinuum generation in photonic crystal fiber," *Rev. Mod. Phys.* **78**, 1135–1184 (2006).
4. D. V. Skryabin and A. V. Gorbach, "Looking at a soliton through the prism of optical supercontinuum," *Rev. Mod. Phys.* **82**, 1287–1299 (2010).
5. G. P. Agrawal, *Nonlinear Fiber Optics*, 5th ed. (Academic, 2013).
6. F. Lu, Q. Lin, W. H. Knox, and G. P. Agrawal, "Vector soliton fission," *Phys. Rev. Lett.* **93**, 183901 (2004).
7. E. R. Martins, D. H. Spadoti, M. A. Romero, and B.-H. V. Borges, "Theoretical analysis of supercontinuum generation in a highly birefringent D-shaped microstructured optical fiber," *Opt. Express* **15**, 14335–14347 (2007).
8. H. Tu, Y. Liu, X. Liu, D. Turchinovich, J. Lagsgaard, and S. A. Boppart, "Nonlinear polarization dynamics in a weakly birefringent all-normal dispersion photonic crystal fiber: toward a practical coherent fiber supercontinuum laser," *Opt. Express* **20**, 1113–1128 (2012).
9. R. C. Herrera and C. T. Law, "Dispersive waves in birefringent nonlinear fiber optics," *Opt. Eng.* **52**, 015007 (2013).
10. A. V. Yulin, L. R. Gorbão, R. Driben, and D. V. Skryabin, "Tuning resonant interaction of orthogonally polarized solitons and dispersive waves with the soliton power," *Opt. Express* **22**, 10995–11000 (2014).
11. K. J. Blow and D. Wood, "Theoretical description of transient stimulated Raman scattering in optical fibers," *IEEE J. Quantum Electron.* **25**, 2665–2673 (1989).

12. S. Trillo and S. Wabnitz, "Parametric and Raman amplification in birefringent fibers," *J. Opt. Soc. Am. B* **9**, 1061–1082 (1992).
13. Q. Lin and G. P. Agrawal, "Raman response function for silica fibers," *Opt. Lett.* **31**, 3086–3088 (2006).
14. T. Ueda and W. L. Kath, "Dynamics of coupled solitons in nonlinear optical fibers," *Phys. Rev. A* **42**, 563–571 (1990).
15. C. R. Menyuk, "Stability of solitons in birefringent optical fibers. II. Arbitrary amplitudes," *J. Opt. Soc. Am. B* **5**, 392–402 (1988).
16. J. M. Dudley and J. R. Taylor, *Supercontinuum Generation in Optical Fibers* (Cambridge University, 2010), Chap. 8.
17. W. Yang, J. P. Snyder, and W. Tobler, *Map Projection Transformation: Principles and Applications* (CRC Press, 1999).
18. D. V. Skryabin and A. V. Yulin, "Theory of generation of new frequencies by mixing of solitons and dispersive waves in optical fibers," *Phys. Rev. E* **72**, 016619 (2005).
19. B. Daino, G. Gregori, and S. Wabnitz, "New all-optical devices based on third-order nonlinearity of birefringent fibers," *Opt. Lett.* **11**, 42–44 (1986).
20. S. Trillo, S. Wabnitz, R. H. Stolen, G. Assanto, C. T. Seaton, and G. I. Stegeman, "Experimental observation of polarization instability in a birefringent optical fiber," *Appl. Phys. Lett.* **49**, 1224–1226 (1986).
21. M. Conforti and S. Trillo, "Dispersive wave emission from wave breaking," *Opt. Lett.* **38**, 3815–3818 (2013).